FIERY: Future Instance Prediction in Bird's-Eye View from Surround Monocular Cameras

Anthony Hu[1,2] Zak Murez[1] Nikhil Mohan[1] Sofía Dudas[1]
Jeff Hawke[1] Vijay Badrinarayanan[1] Roberto Cipolla[2] Alex Kendall[1]

[1]Wayve, UK. [2]University of Cambridge, UK.

Abstract

Driving requires interacting with road agents and predicting their future behaviour in order to navigate safely. We present FIERY: a probabilistic future prediction model in bird's-eye view from monocular cameras. Our model predicts future instance segmentation and motion of dynamic agents that can be transformed into non-parametric future trajectories. Our approach combines the perception, sensor fusion and prediction components of a traditional autonomous driving stack by estimating bird's-eye-view prediction directly from surround RGB monocular camera inputs. FIERY learns to model the inherent stochastic nature of the future directly from camera driving data in an end-to-end manner, without relying on HD maps, and predicts multimodal future trajectories. We show that our model outperforms previous prediction baselines on the NuScenes and Lyft datasets.[1]

1. Introduction

Prediction of future states is a key challenge in many autonomous decision making systems. This is particularly true for motion planning in highly dynamic environments: for example in autonomous driving where the motion of other road users and pedestrians has a substantial influence on the success of motion planning [10]. Estimating the motion and future poses of these road users enables motion planning algorithms to better resolve multimodal outcomes where the optimal action may be ambiguous knowing only the current state of the world.

Autonomous driving is inherently a geometric problem, where the goal is to navigate a vehicle safely and correctly through 3D space. As such, an orthographic bird's-eye view (BEV) perspective is commonly used for motion planning and prediction based on LiDAR sensing [38, 49]. Recent advances in camera-based perception have rivalled LiDAR-based perception [48], and we anticipate that this will also be possible for wider monocular vision tasks, including prediction. Building a perception and prediction system based on cameras would enable a leaner, cheaper and higher resolution visual recognition system over LiDAR sensing.

Most of the work in camera-based prediction to date has either been performed directly in the perspective view coordinate frame [1, 23], or using simplified BEV raster representations of the scene [28, 12, 10] generated by HD-mapping systems such as [29, 16]. We wish to build predictive models that operate in an orthographic bird's-eye view frame (due to the benefits for planning and control [34]), though *without* relying on auxiliary systems to generate a BEV raster representation of the scene.

A key theme in robust perception systems for autonomous vehicles has been the concept of early sensor fusion, generating 3D object detections directly from image and LiDAR data rather than seeking to merge the predicted outputs of independent object detectors on each sensor input. Learning a task jointly from multiple sources of sensory data as in [50], rather than a staged pipeline, has been demonstrated to offer improvement to perception performance in tasks such as object detection. We seek similar benefits in joining perception and sensor fusion to prediction by estimating bird's-eye-view prediction directly from surround RGB monocular camera inputs, rather than a multi-stage discrete pipeline of tasks.

Further, traditional autonomous driving stacks [13] tackle future prediction by extrapolating the current behaviour of dynamic agents, without taking into account possible interactions. They rely on HD maps and use road connectivity to generate a set of future trajectories. FIERY learns to predict future motion of road agents directly from camera driving data in an end-to-end manner, without relying on HD maps. It can reason about the probabilistic nature of the future, and predicts multimodal future trajectories (see blog post and Figure 1).

To summarise the main contributions of this paper:

[1]Code is available at https://github.com/wayveai/fiery.

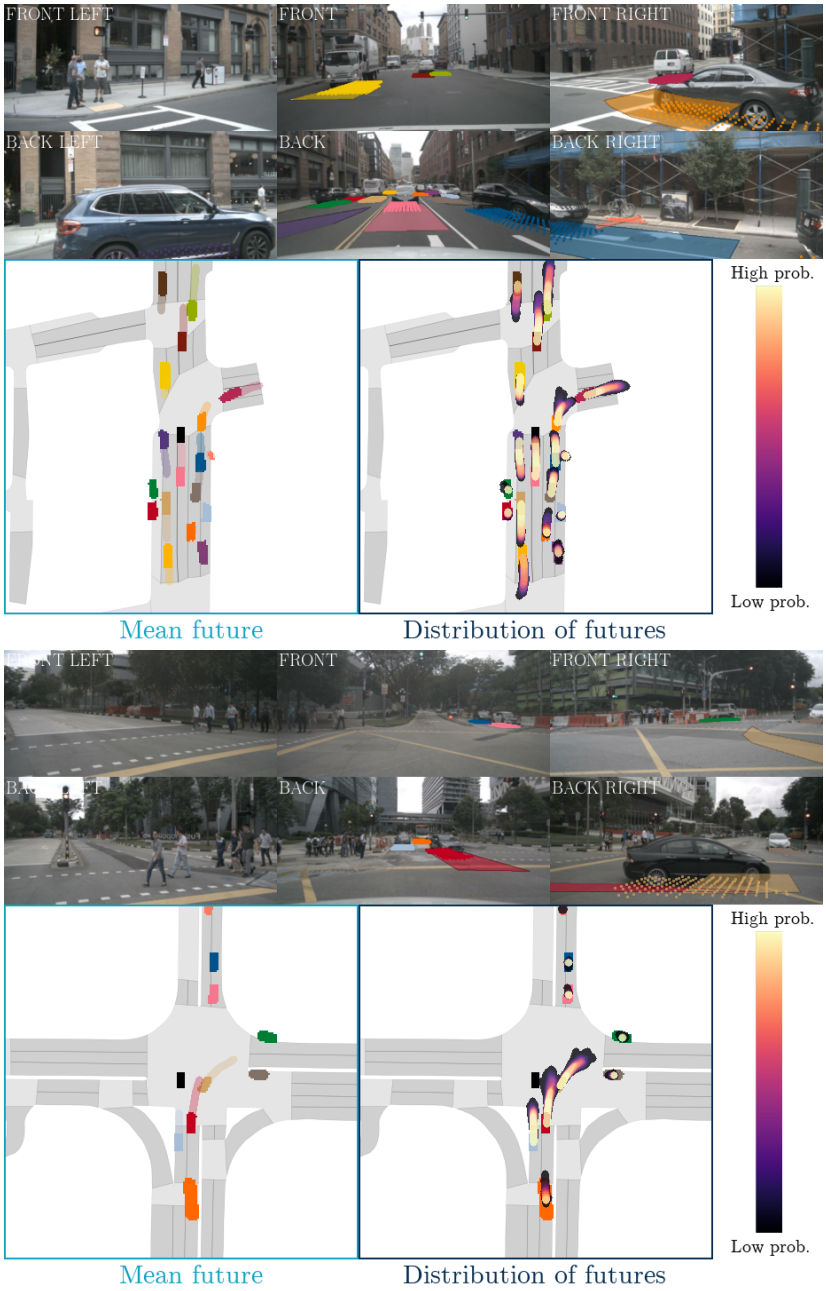

Figure 1: Multimodal future predictions by our bird's-eye view network. Top two rows: RGB camera inputs. The predicted instance segmentations are projected to the ground plane in the images. We also visualise the mean future trajectory of dynamic agents as transparent paths. Bottom row: future instance prediction in bird's-eye view in a $100\text{m} \times 100\text{m}$ capture size around the ego-vehicle, which is indicated by a black rectangle in the center.

1. We present the first future prediction model in bird's-eye view from monocular camera videos. Our framework explicitly reasons about multi-agent dynamics by predicting temporally consistent future instance segmentation and motion in bird's-eye view.
2. Our probabilistic model predicts plausible and multi-modal futures of the dynamic environment.
3. We demonstrate quantitative benchmarks for future dynamic scene segmentation, and show that our learned prediction outperforms previous prediction baselines for autonomous driving on the NuScenes [5] and Lyft [25] datasets.

2. Related Work

Bird's-eye view representation from cameras. Many prior works [51, 47] have tackled the inherently ill-posed problem [17] of lifting 2D perspective images into a bird's-eye view representation. [35, 33] dealt specifically with the problem of generating semantic BEV maps directly from images and used a simulator to obtain the ground truth.

Recent multi-sensor datasets, such as NuScenes [5] or Lyft [25], made it possible to directly supervise models on real-world data by generating bird's-eye view semantic segmentation labels from 3D object detections. [39] proposed a Bayesian occupancy network to predict road elements and dynamic agents in BEV directly from monocular RGB images. Most similar to our approach, Lift-Splat [37] learned a depth distribution over pixels to lift camera images to a 3D point cloud, and project the latter into BEV using camera geometry. Fishing Net [19] tackled the problem of predicting deterministic future bird's-eye view semantic segmentation using camera, radar and LiDAR inputs.

Future prediction. Classical methods for future prediction generally employ a multi-stage detect-track-predict paradigm for trajectory prediction [8, 20, 46]. However, these methods are prone to cascading errors and high latency, and thus many have turned to an end-to-end approach for future prediction. Most end-to-end approaches rely heavily on LiDAR data [32, 11], showing improvements by incorporating HD maps [7], encoding constraints [6], and fusing radar and other sensors for robustness [43]. These end-to-end methods are faster and have higher performance as compared to the traditional multi-stage approaches.

The above methods attempt future prediction by producing a single deterministic trajectory [7, 19], or a single distribution to model the uncertainty of each waypoint of the trajectory [6, 11]. However, in the case of autonomous driving, one must be able to anticipate a range of behaviors for actors in the scene, jointly. From an observed past, there are many valid and probable futures that could occur [21]. Other work [8, 46, 36] has been done on probabilistic multi-hypothesis trajectory prediction, however all assume access to top-down rasterised representations as inputs. Our approach is the first to predict diverse and plausible future vehicle trajectories directly from raw camera video inputs.

3. Model Architecture

An overview of our model is given in Figure 2.

3.1. Lifting camera features to 3D

For every past timestep, we use the method of [37] to extract image features from each camera and then lift and fuse them into a BEV feature map. In particular, each image is passed through a standard convolutional encoder E (we use EfficientNet [45] in our implementation) to obtain a set of features to be lifted and a set of discrete depth probabilities. Let $O_t = \{I_t^1, ..., I_t^n\}$ be the set of $n = 6$ camera images at time t. We encode each image I_t^k with the encoder: $e_t^k = E(I_t^k) \in \mathbb{R}^{(C+D)\times H_e \times W_e}$, with C the number of feature channels, D the number of discrete depth values and (H_e, W_e) the feature spatial size. D is equal to the number of equally spaced depth slices between D_{min} (the minimum depth value) and D_{max} (the maximum depth value) with size $D_{\text{size}} = 1.0\text{m}$. Let us split this feature into two: $e_t^k = (e_{t,C}^k, e_{t,D}^k)$ with $e_{t,C}^k \in \mathbb{R}^{C\times H_e \times W_e}$ and $e_{t,D}^k \in \mathbb{R}^{D\times H_e \times W_e}$. A tensor $u_t^k \in \mathbb{R}^{C\times D\times H_e \times W_e}$ is formed by taking the outer product of the features to be lifted with the depth probabilities:

$$u_t^k = e_{t,C}^k \otimes e_{t,D}^k \tag{1}$$

The depth probabilities act as a form of self-attention, modulating the features according to which depth plane they are predicted to belong to. Using the known camera intrinsics and extrinsics (position of the cameras with respect to the center of gravity of the vehicle), these tensors from each camera $(u_t^1, ..., u_t^n)$ are lifted to 3D in a common reference frame (the inertial center of the ego-vehicle at time t).

3.2. Projecting to bird's-eye view

In our experiments, to obtain a bird's-eye view feature, we discretise the space in $0.50\text{m} \times 0.50\text{m}$ columns in a $100\text{m} \times 100\text{m}$ capture size around the ego-vehicle. The 3D features are sum pooled along the vertical dimension to form bird's-eye view feature maps $x_t \in \mathbb{R}^{C\times H\times W}$, with $(H, W) = (200, 200)$ the spatial extent of the BEV feature.

3.3. Learning a temporal representation

The past bird's-eye view features $(x_1, ..., x_t)$ are transformed to the present's reference frame (time t) using known past ego-motion $(a_1, ..., a_{t-1})$. $a_{t-1} \in SE(3)$ corresponds to the ego-motion from $t-1$ to t, i.e. the translation and rotation of the ego-vehicle. Using a Spatial Transformer [22] module S, we warp past features x_i to the present for $i \in \{1, ..., t-1\}$:

$$x_i^t = S(x_i, a_{t-1} \cdot a_{t-2} \cdot ... \cdot a_i) \tag{2}$$

Since we lose the past ego-motion information with this operation, we concatenate spatially-broadcast actions to the warped past features x_i^t.

These features are then the input to a temporal model $\mathcal{T}$ which outputs a spatio-temporal state s_t:

$$s_t = \mathcal{T}(x_1^t, x_2^t, ..., x_t^t) \tag{3}$$

with $x_t^t = x_t$. $\mathcal{T}$ is a 3D convolutional network with local spatio-temporal convolutions, global 3D pooling lay-

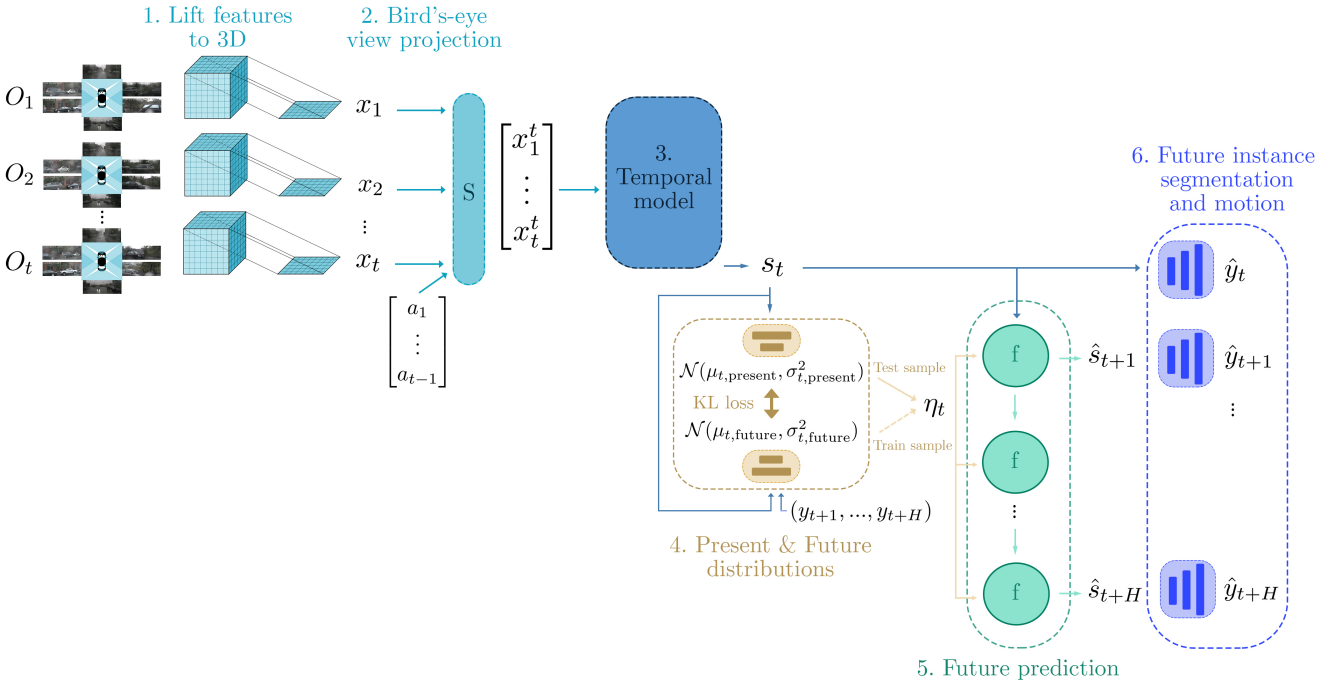

Figure 2: The architecture of FIERY: a future prediction model in bird's-eye view from camera inputs.

1. At each past timestep $\{1, ..., t\}$, we lift camera inputs $(O_1, ..., O_t)$ to 3D by predicting a depth probability distribution over pixels and using known camera intrinsics and extrinsics.
2. These features are projected to bird's-eye view $(x_1, ..., x_t)$. Using past ego-motion $(a_1, ..., a_{t-1})$, we transform the bird's-eye view features into the present reference frame (time t) with a Spatial Transformer module S.
3. A 3D convolutional temporal model learns a spatio-temporal state s_t.
4. We parametrise two probability distributions: the present and the future distribution. The present distribution is conditioned on the current state s_t, and the future distribution is conditioned on both the current state s_t and future labels $(y_{t+1}, ..., y_{t+H})$.
5. We sample a latent code η_t from the future distribution during training, and from the present distribution during inference. The current state s_t and the latent code η_t are the inputs to the future prediction model that recursively predicts future states $(\hat{s}_{t+1}, ..., \hat{s}_{t+H})$.
6. The states are decoded into future instance segmentation and future motion in bird's-eye view $(\hat{y}_t, ..., \hat{y}_{t+H})$.

ers, and skip connections. For more details, please see Appendix B.

3.4. Present and future distributions

Following [21] we adopt a conditional variational approach to model the inherent stochasticity of future prediction. We introduce two distributions: a *present distribution* P which only has access to the current spatio-temporal state s_t, and a *future distribution* F that additionally has access to the observed future labels $(y_{t+1}, ..., y_{t+H})$, with H the future prediction horizon. The labels correspond to future centerness, offset, segmentation, and flow (see Section 3.6).

We parametrise both distributions as diagonal Gaussians with mean $\mu \in \mathbb{R}^L$ and variance $\sigma^2 \in \mathbb{R}^L$, L being the latent dimension. During training, we use samples $\eta_t \sim \mathcal{N}(\mu_{t,\text{future}}, \sigma^2_{t,\text{future}})$ from the future distribution to enforce predictions consistent with the observed future, and a mode covering Kullback-Leibler divergence loss to encourage the present distribution to cover the observed futures:

$$L_{\text{probabilistic}} = D_{\text{KL}}(F(\cdot|s_t, y_{t+1}, ..., y_{t+H}) \,||\, P(\cdot|s_t)) \quad (4)$$

During inference, we sample $\eta_t \sim \mathcal{N}(\mu_{t,\text{present}}, \sigma^2_{t,\text{present}})$ from the present distribution where each sample encodes a possible future.

3.5. Future prediction in bird's-eye view

The future prediction model is a convolutional gated recurrent unit network taking as input the current state s_t and the latent code η_t sampled from the future distribution F during training, or the present distribution P for inference. It recursively predicts future states $(\hat{s}_{t+1}, ..., \hat{s}_{t+H})$.

(a) Camera inputs.

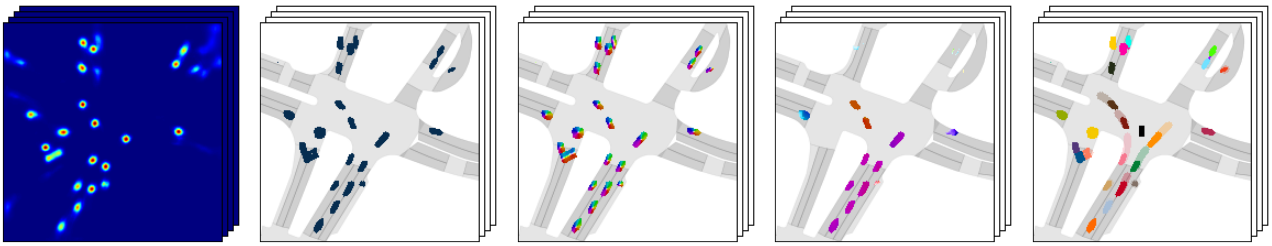

(b) Centerness. (c) Segmentation. (d) Offset. (e) Future flow. (f) Instance segmentation.

Figure 3: Outputs from our model. (b) shows a heatmap of instance centerness and indicates the probability of finding an instance center (from blue to red). (c) represents the vehicles segmentation. (d) shows a vector field indicating the direction to the instance center. (e) corresponds to future motion – notice how consistent the flow is for a given instance, since it's a rigid-body motion. (f) shows the final output of our model: a sequence of temporally consistent future instance segmentation in bird's-eye view where: (i) Instance centers are obtained by non-maximum suppression. (ii) The pixels are then grouped to their closest instance center using the offset vector. (iii) Future flow allows for consistent instance identification by comparing the warped centers using future flow from t to $t+1$, and the centers at time $t+1$. The ego-vehicle is indicated by a black rectangle.

3.6. Future instance segmentation and motion

The resulting features are the inputs to a bird's-eye view decoder $\mathcal{D}$ which has multiple output heads: semantic segmentation, instance centerness and instance offset (similarily to [9]), and future instance flow. For $j \in \{0, ..., H\}$:

$$\hat{y}_{t+j} = \mathcal{D}(\hat{s}_{t+j}) \tag{5}$$

with $\hat{s}_t = s_t$.

For each future timestep j, the instance centerness indicates the probability of finding an instance center (see Figure 3b). By running non-maximum suppression, we get a set of instance centers. The offset is a vector pointing to the center of the instance (Figure 3d), and can be used jointly with the segmentation map (Figure 3c) to assign neighbouring pixels to its nearest instance center and form the bird's-eye view instance segmentation (Figure 3f). The future flow (Figure 3e) is a displacement vector field of the dynamic agents. It is used to consistently track instances over time by comparing the flow-warped instance centers at time $t+j$ and the detected instance centers at time $t+j+1$ and running a Hungarian matching algorithm [27].

A full description of our model is given in Appendix B.

3.7. Losses

For semantic segmentation, we use a top-k cross-entropy loss [48]. As the bird's-eye view image is largely dominated by the background, we only backpropagate the top-k hardest pixels. In our experiments, we set $k = 25\%$. The centerness loss is a L_2 distance, and both offset and flow losses are L_1 distances. We exponentially discount future timesteps with a parameter $\gamma = 0.95$.

4. Experimental Setting

4.1. Dataset

We evaluate our approach on the NuScenes [5] and Lyft [25] datasets. NuScenes contains 1000 scenes, each 20 seconds in length, annotated at 2Hz. The Lyft dataset contains 180 scenes, each $25-45$ seconds in length, annotated at 5Hz. In both datasets, the camera rig covers the full 360° field of view around the ego-vehicle, and is comprised of 6 cameras with a small overlap in field of view. Camera intrinsics and extrinsics are available for each camera in every scene.

The labels $(y_t, ..., y_{t+H})$ are generated by projecting the provided 3D bounding boxes of vehicles into the bird's-eye view plane to create a bird's-eye view occupancy grid. See

Appendix B.2 for more detail. All the labels $(y_t, ..., y_{t+H})$ are in the present's reference frame and are obtained by transforming the labels with the ground truth future ego-motion.

4.2. Metrics

Future Video Panoptic Quality. We want to measure the performance of our system in both:

(i) Recognition quality: how consistently the instances are detected over time.
(ii) Segmentation quality: how accurate the instance segmentations are.

We use the *Video Panoptic Quality* (VQP) [26] metric defined as:

$$\text{VPQ} = \sum_{t=0}^{H} \frac{\sum_{(p_t,q_t)\in TP_t} \text{IoU}(p_t, q_t)}{|TP_t| + \frac{1}{2}|FP_t| + \frac{1}{2}|FN_t|} \tag{6}$$

with TP_t the set of true positives at timestep t (correctly detected ground truth instances), FP_t the set of false positives at timestep t (predicted instances that do not match any ground truth instance), and FN_t the set of false negatives at timestep t (ground truth instances that were not detected). A true positive corresponds to a predicted instance segmentation that has: (i) an intersection-over-union (IoU) over 0.5 with the ground truth, and (ii) an instance id that is consistent with the ground truth over time (correctly tracked).

Generalised Energy Distance. To measure the ability of our model to predict multi-modal futures, we report the *Generalised Energy Distance* (D_{GED}) [44]. Let $(\hat{Y}, \hat{Y}')$ be samples of predicted futures from our model, (Y, Y') be samples of ground truth futures and d be a distance metric. D_{GED} is defined as:

$$D_{\text{GED}} = 2\mathbb{E}[d(\hat{Y}, Y)] - \mathbb{E}[d(\hat{Y}, \hat{Y}')] - \mathbb{E}[d(Y, Y')] \tag{7}$$

We set our distance metric d to $d(x, y) = 1 - \text{VPQ}(x, y)$. Since we only have access to a unique ground truth future Y, the Generalised Energy Distance simplifies to:

$$D_{\text{GED}} = 2\mathbb{E}[d(\hat{Y}, Y)] - \mathbb{E}[d(\hat{Y}, \hat{Y}')] \tag{8}$$

4.3. Training

Our model takes 1.0s of past context and predicts 2.0s in the future. In NuScenes, this corresponds to 3 frames of past temporal context and 4 frames into the future at 2Hz. In the Lyft dataset, this corresponds to 6 frames of past context and 10 frames in the future at 5Hz.

For each past timestep, our model processes 6 camera images at resolution 224×480. It outputs a sequence of $100\text{m} \times 100\text{m}$ BEV predictions at 50cm pixel resolution in both the x and y directions resulting in a bird's-eye view video with spatial dimension 200×200. We use the Adam optimiser with a constant learning rate of 3×10^{-4}. We train our model on 4 Tesla V100 GPUs with a batch size of 12 for 20 epochs at mixed precision.

5. Results

5.1. Comparison to the literature

Since predicting future instance segmentation in bird's-eye view is a new task, we begin by comparing our model to previous published methods on bird's-eye view semantic segmentation from monocular cameras.

Many previous works [30, 35, 39, 37, 42] have proposed a model to output the dynamic scene bird's-eye view segmentation from multiview camera images of a single timeframe. For comparison, we adapt our model so that the past context is reduced to a single observation, and we set the future horizon $H = 0$ (to only predict the present's segmentation). We call this model *FIERY Static* and report the results in Table 1. We observe that FIERY Static outperforms all previous baselines.

	Intersection-over-Union (IoU)		
	Setting 1	Setting 2	Setting 3
VED [30]	8.8	-	-
PON [39]	24.7	-	-
VPN [35]	25.5	-	-
STA [42]	36.0	-	-
Lift-Splat [37]	-	32.1	-
Fishing Camera [19]	-	-	30.0
Fishing Lidar [19]	-	-	44.3
FIERY Static	39.9	36.7	-
FIERY	**41.1**	**38.2**	**58.5**

Table 1: Bird's-eye view semantic segmentation on NuScenes in the settings of the respective published methods.
Setting 1: $100\text{m} \times 50\text{m}$ at 25cm resolution. Prediction of the present timeframe.
Setting 2: $100\text{m} \times 100\text{m}$ at 50cm resolution. Prediction of the present timeframe.
Setting 3: $32.0\text{m} \times 19.2\text{m}$ at 10cm resolution. Prediction 2.0s in the future. In this last setting we compare our model to two variants of Fishing Net [19]: one using camera inputs, and one using LiDAR inputs.

We also train a model that takes 1.0s of past observations as context (*FIERY*) and note that it achieves an even higher intersection-over-union over its single-timeframe counterpart that has no past context. We hypothesise this is due to our model's ability to accumulate information over time and

Figure 4: Qualitative comparison of bird's-eye view prediction with published methods. The predictions of our model are much sharper and more accurate. Contrary to previous methods, FIERY can separate closely parked cars and correctly predict distant vehicles (i.e. $> 40\text{m}$, near the top of the bird's-eye view image).

better handle partial observability and occlusions. Qualitatively, as shown in Figure 4, our predictions are much sharper and more accurate.

Finally, we compare our model to Fishing Net [19], where the authors predicts bird's-eye view semantic segmentation 2.0s in the future. Fishing Net proposes two variants of their model: one using camera as inputs, and one using LiDAR as inputs. FIERY performs much better than both the camera and LiDAR models, hinting that computer vision networks are starting to become competitive with LiDAR sensing for the prediction task.

5.2. Future instance prediction

In order to compare the performance of our model for future instance segmentation and motion prediction, we introduce the following baselines:

Static model. The most simple approach to model dynamic obstacles is to assume that they will not move and remain static. We use FIERY Static to predict the instance segmentation of the present timestep (time t), and repeat this prediction in the future. We call this baseline the *Static model* as it should correctly detect all static vehicles, since the future labels are in the present's reference frame.

Extrapolation model. Classical prediction methods [14, 15] extrapolate the current behaviour of dynamic agents in the future. We run FIERY Static on every past timesteps to obtain a sequence of past instance segmentations. We re-identify past instances by comparing the instance centers and running a Hungarian matching algorithm. We then obtain past trajectories of detected vehicles, which we extrap-

	Intersection-over-Union		Video Panoptic Quality	
	Short	Long	Short	Long
Static model	47.9	30.3	43.1	24.5
Extrapolation model	49.2	30.8	43.8	24.9
No temporal context	51.7	32.6	40.3	24.1
No transformation	53.0	33.8	41.7	24.6
No unrolling	55.4	34.9	44.2	26.2
No future flow	58.0	36.7	44.6	26.9
Uniform depth	57.1	36.2	46.8	27.8
Deterministic	58.2	36.6	48.3	28.5
FIERY	**59.0**	**37.0**	**49.7**	**29.5**

Table 2: Future instance segmentation in bird's-eye view for 2.0s in the future on NuScenes. We report future Intersection-over-Union (IoU) and Video Panoptic Quality (VPQ), evaluated at different ranges: $30\text{m} \times 30\text{m}$ (Short) and $100\text{m} \times 100\text{m}$ (Long) around the ego-vehicle. Results are reported as percentages.

olate in the future and transform the present segmentation accordingly.

We also report the results of various ablations of our proposed architecture:

- **No temporal context.** This model only uses the features x_t from the present timestep to predict the future (*i.e.* we set the 3D convolutional temporal model to the identity function).
- **No transformation.** Past bird's-eye view features $(x_1, ..., x_t)$ are not warped to the present's reference frame.
- **No future flow.** This model does not predict future flow.
- **No unrolling.** Instead of recursively predicting the next states $\hat{s}_{t+j}$ and decoding the corresponding instance information $\hat{y}_{t+j} = \mathcal{D}(\hat{s}_{t+j})$, this variant directly predicts all future instance centerness, offset, segmentation and flow from s_t.
- **Uniform depth.** We lift the features from the encoder $(e_t^1, ..., e_t^n)$ with the Orthographic Feature Transform [40] module. This corresponds to setting the depth probability distribution to a uniform distribution.
- **Deterministic.** We remove the probabilistic modelling.

We report the results in Table 2 (on NuScenes) and Table 3 (on Lyft) of the mean prediction of our probabilistic model (i.e. we set the latent code η_t to the mean of the present distribution: $\eta_t = \mu_{t,\text{present}}$).

5.3. Analysis

FIERY largely outperforms the Static and Extrapolation baselines for the task of future prediction. Figure 5 shows the performance boost our model gains from different parts of the model.

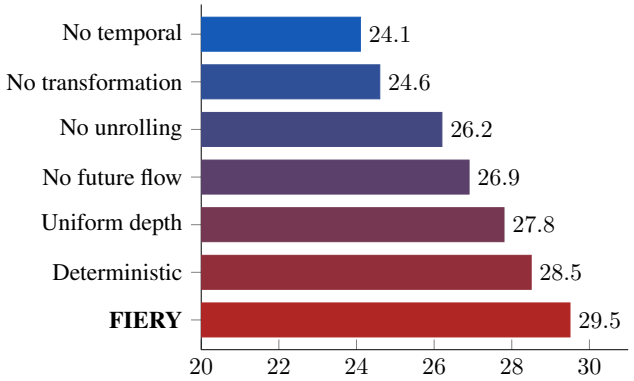

Figure 5: Performance comparison of various ablations of our model. We measure future Video Panoptic Quality 2.0s in the future on NuScenes.

Temporal model. The *No temporal context* variant performs similarly to the static model. That is to be expected as this model does not have any information from the past, and cannot infer much about the motion of road agents.

Transformation to the present's reference frame. There is a large performance drop when we do not transform past features to the present's reference frame. This can be explained by how much easier it is for the temporal model to learn correspondences between dynamic vehicles when the ego-motion is factored out.

Past prediction models either naively fed past images to a temporal model [4, 21], or did not use a temporal model altogether and simply concatenated past features [31, 19]. We believe that in order to learn temporal correspondences, past features have to be mapped to a common reference frame and fed into a high capacity temporal model, such as our proposed 3D convolutional architecture.

	IoU|VPQ	
	Short	Long
Static model	35.3|36.4	24.1|20.7
Extrapolation model	37.4|37.5	24.8|21.2
FIERY	**58.1|49.9**	**36.6|29.5**

Table 3: Future instance prediction in bird's-eye view for 2.0s in the future on the Lyft dataset. We report future Intersection-over-Union and Video Panoptic Quality.

Predicting future states. When predicting the future, it is important to model its sequential nature, i.e. the prediction at time $t+j+1$ should be conditioned on the prediction at time $t+j$.

The *No unrolling* variant which directly predicts all future instance segmentations and motions from the current state s_t, results in a large performance drop. This is because the sequential constraint is no longer enforced, contrarily to our approach that predicts future states in a recursive way.

Future motion. Learning to predict future motion allows our model to re-identify instances using the predicted flow and comparing instance centers. Our model is the first to produce temporally consistent future instance segmentation in bird's-eye view of dynamic agents. Without future flow, the predictions are no longer temporally consistent explaining the sharp decrease in performance.

Lifting the features to 3D Using a perfect depth model we could directly lift each pixel to its correct location in 3D space. Since our depth prediction is uncertain, we instead lift the features at different possible depth locations and assign a probability mass at each location, similar to [37]. The *Uniform depth* baseline uses the Orthographic Feature Transform to lift features in 3D, by setting a uniform distribution on all depth positions. We observe that such a naive lifting performs worse compared to a learned weighting over depth.

Present and future distributions. A deterministic model has a hard task at hand. It has to output with full confidence which future will happen, even though the said future is uncertain. In our probabilistic setting, the model is guided during training with the future distribution that outputs a latent code that indicates the correct future. It also encourages the present distribution to cover the modes of the future distribution. This paradigm allows FIERY to predict both accurate and diverse futures as we will see in section Section 5.4.

Further analyses on understanding the structure of the learned space and on the temporal horizon of future prediction is available in Appendix A.

5.4. Probabilistic modelling

We compare our probabilistic future prediction model to the following baselines:

- **M-Head.** The M-head model inspired by [41] outputs M different futures. During training, the best performing head backpropagates its loss with weight $(1-\epsilon)$ while the other heads are weighted by $\frac{\epsilon}{M-1}$. We set $\epsilon = 0.05$.
- **Bayesian Dropout.** We insert a dropout layer after every 3D temporal convolution in the temporal model. We also insert a dropout layer in the first 3 layers of the decoder, similarly to [2]. We set the dropout parameter to $p = 0.25$.
- **Classical VAE.** We use a Centered Unit Gaussian to constrain our probability distribution similarly to the technique used in [3]. Different latent codes are sampled from $\mathcal{N}(0, I_L)$ during inference.

We report the results in Table 4.

	Generalised Energy Distance (↓)	
	Short	Long
M-Head	96.6	122.3
Bayesian Dropout	92.5	116.5
Classical VAE	93.2	109.6
FIERY	**90.5**	**105.1**

Table 4: Generalised Energy Distance on NuScenes, for 2.0s future prediction and $M = 10$ samples, showing that our model is able to predict the most accurate and diverse futures.

6. Conclusion

Autonomous driving requires decision making in multimodal scenarios, where the present state of the world is not always sufficient to reason correctly alone. Predictive models estimating the future state of the world – particularly other dynamic agents – are therefore a key component to robust driving. We presented the first prediction model of dynamic agents for autonomous driving in bird's-eye view from surround RGB videos. We posed this as an end-to-end learning problem in which our network models future stochasticity with a variational distribution. We demonstrated that FIERY predicts temporally consistent future instance segmentations and motion and is able to model diverse futures accurately. In future work, we would like to jointly train a driving policy to condition the future prediction model on future actions. Such a framework would enable effective motion planning in a model-based reinforcement learning setting.

A. Additional Results

A.1. Visualisation of the learned states

We run a Principal Component Analysis on the states s_t and a Gaussian Mixture algorithm on the projected features in order to obtain clusters. We then visualise the inputs and predictions of the clusters in Figures 6, 8 and 9. We observe that examples in a given cluster correspond to similar scenarios. Therefore, we better understand why our model is able to learn diverse and multimodal futures from a deterministic training dataset. Since similar scenes are mapped to the same state s_t, our model will effectively observe different futures starting from the same initial state. The present distribution will thus learn to capture the different modes in the future.

A.2. Temporal horizon of future prediction

Figure 7 shows the performance of our model for different temporal horizon: from 1.0s to 8.0s in the future. The performance seems to plateau beyond 6.0s in the future. In such a large future horizon, the prediction task becomes increasingly difficult as (i) uncertainty in the future grows further in time, and (ii) dynamic agents might not even be visible from past frames.

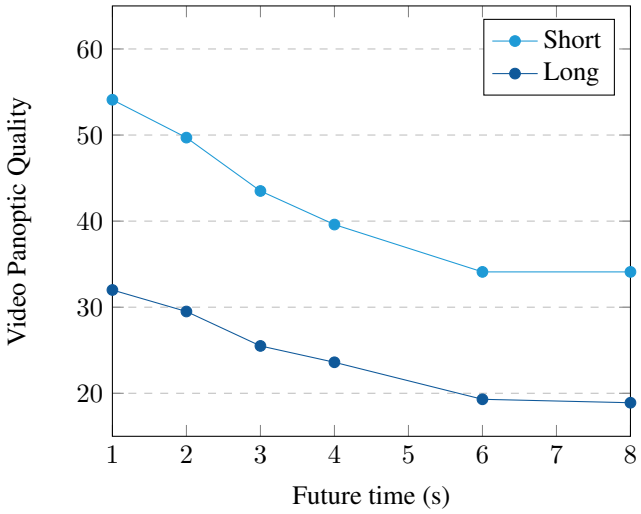

Figure 7: Future prediction performance for different temporal horizons. We report future Video Panoptic Quality on NuScenes at different capture sizes around the ego-car: $30\text{m} \times 30\text{m}$ (Short) and $100\text{m} \times 100\text{m}$ (Long).

(a) Approaching an intersection.

Figure 6: An example of cluster obtained from the spatio-temporal states s_t by running a Gaussian Mixture algorithm on the NuScenes validation set. Our model learns to map similar situations to similar states. Even though the training dataset is deterministic, after mapping the RGB inputs to the state s_t, different futures can be observed from the same starting state. This explains why our probabilistic paradigm can learn to predict diverse and plausible futures.

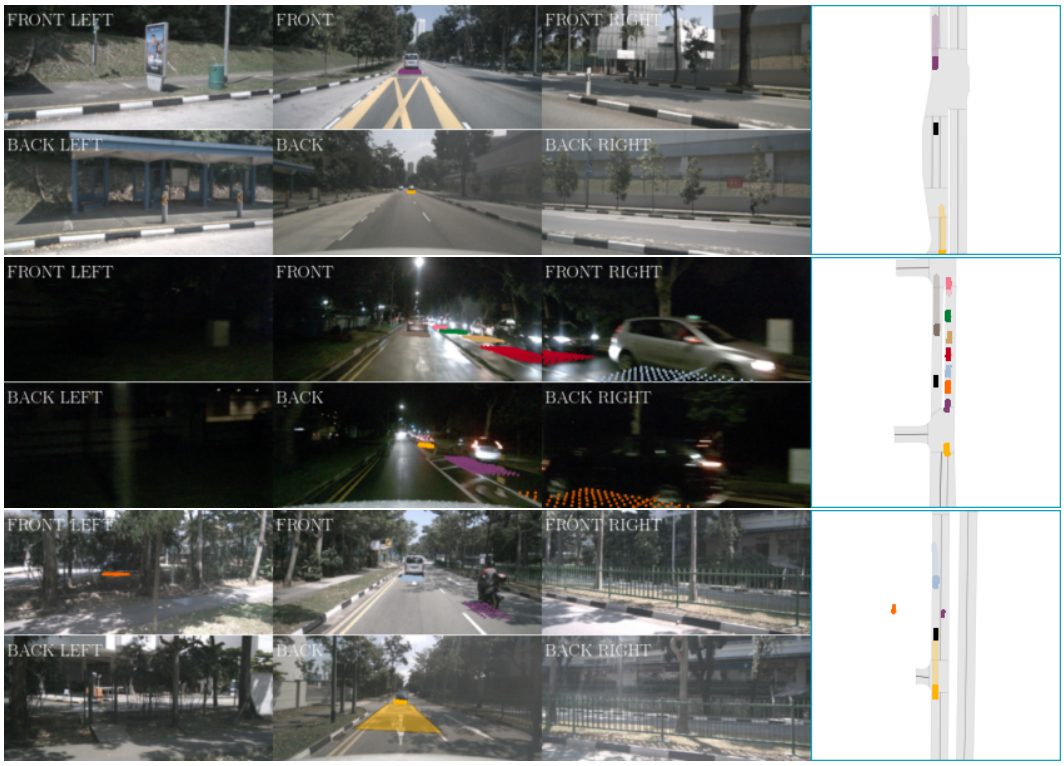

(a) Cruising behind a vehicle.

(b) Driving on open road.

Figure 8: More example of clusters.

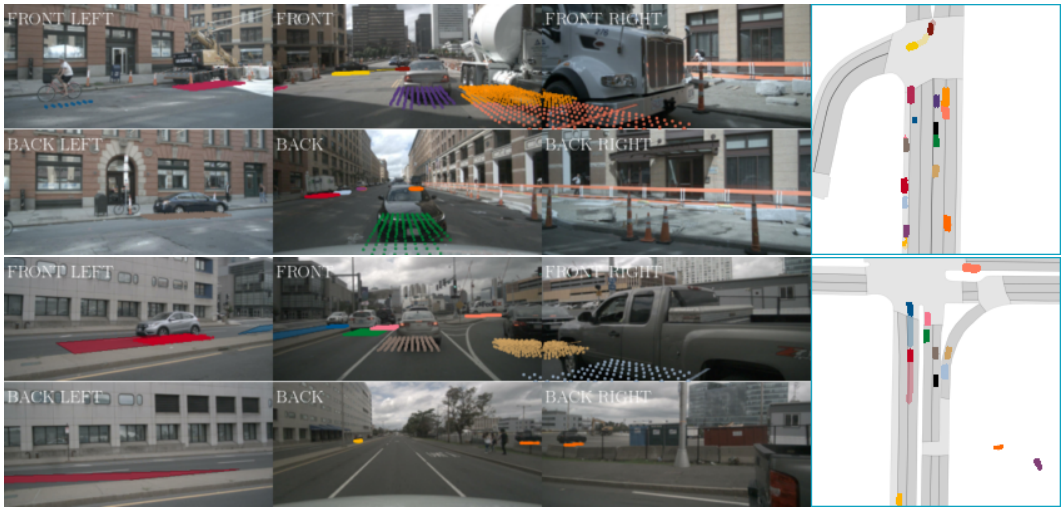

(a) Stuck in traffic.

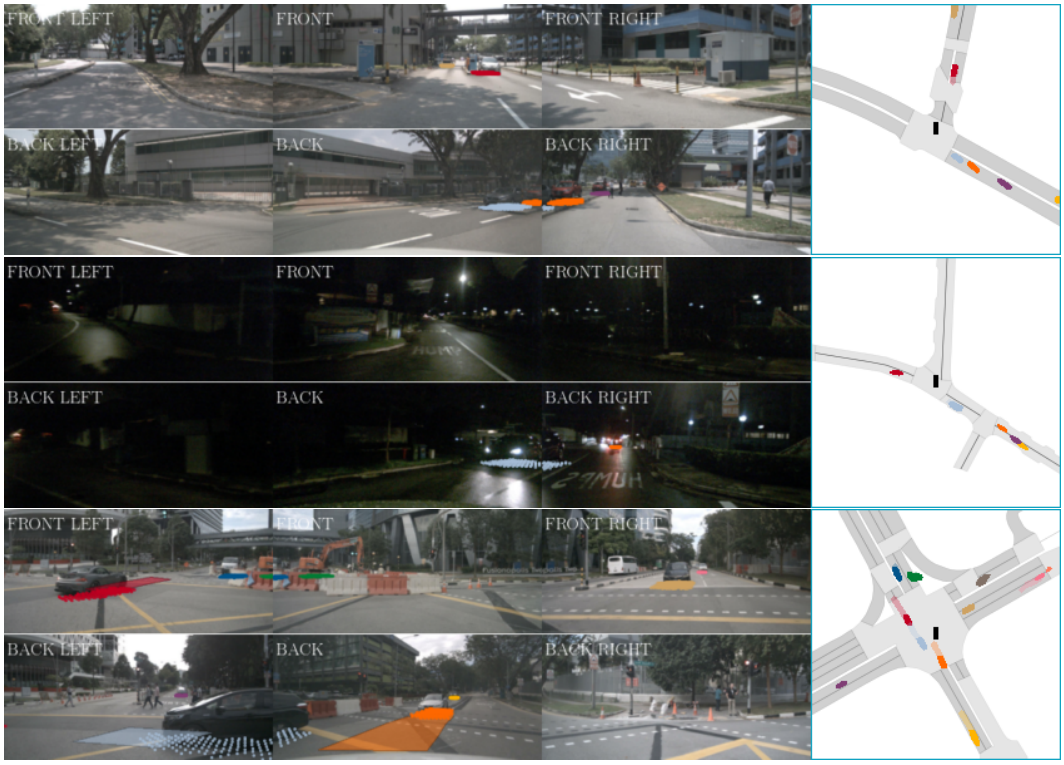

(b) Turning right at an intersection.

Figure 9: More example of clusters.

B. Model and Dataset

B.1. Model description

Our model processes $t = 3$ past observations each with $n = 6$ cameras images at resolution $(H_{\text{in}}, W_{\text{in}}) = (224 \times 480)$, i.e. 18 images. The minimum depth value we consider is $D_{\text{min}} = 2.0\text{m}$, which corresponds to the spatial extent of the ego-car. The maximum depth value is $D_{\text{max}} = 50.0\text{m}$ and the size of each depth slice was set to $D_{\text{size}} = 1.0\text{m}$.

We use uncertainty [24] to weight the segmentation, centerness, offset and flow losses. The probabilistic loss is weighted by $\lambda_{\text{probabilistic}} = 100$.

Our model contains a total of 8.1M parameters and trains in a day on 4 Tesla V100 GPUs with 32GB of memory. All our layers use batch normalisation and a ReLU activation function.

Bird's-eye view encoder. For every past timestep, each image in the observation $O_t = \{I_t^1, ..., I_t^n\}$ is encoded $e_t^k = E(I_t^k) \in \mathbb{R}^{(C+D)\times H_e \times W_e}$. We use the EfficientNet-B4 [45] backbone with an output stride of 8 in our implementation, so $(H_e, W_e) = (\frac{H_{\text{in}}}{8}, \frac{W_{\text{in}}}{8}) = (28, 60)$. The number of channel is $C = 64$ and the number of depth slices is $D = \frac{D_{\text{max}} - D_{\text{min}}}{D_{\text{size}}} = 48$.

These features are then lifted and projected to bird's-eye view to obtain a tensor $x_t \in \mathbb{R}^{C\times H\times W}$ with $(H, W) = (200, 200)$. Using past ego-motion and a spatial transformer module, we transform the bird's-eye view features to the present's reference frame.

Temporal model. The 3D convolutional temporal model is composed of *Temporal Blocks*. Let C_{in} be the number of input channels and C_{out} the number of output channels. A single Temporal block is composed of:

- a 3D convolution, with kernel size $(k_t, k_s, k_s) = (2, 3, 3)$. k_t is the temporal kernel size, and k_s the spatial kernel size.
- a 3D convolution with kernel size $(1, 3, 3)$.
- a 3D global average pooling layer with kernel size $(2, H, W)$.

Each of these operations are preceded by a feature compression layer, which is a $(1, 1, 1)$ 3D convolution with output channels $\frac{C_{\text{in}}}{2}$.

All the resulting features are concatenated and fed through a $(1, 1, 1)$ 3D convolution with output channel C_{out}. The temporal block module also has a skip connection. The final feature $s_t \in \mathbb{R}^{64\times 200\times 200}$.

Present and future distributions. The architecture of the present and future distributions are identical, except for the number of input channels. The present distribution takes as input s_t, and the future distribution takes as input the concatenation of $(s_t, y_{t+1}, ..., y_{t+H})$. Let $C_p = 64$ be the number of input channel of the present distribution and $C_f = 64 + C_y \cdot H = 88$ the number of input channels of the future distribution (since $C_y = 6$ and $H = 4$). The module contains four residual block layers [18] each with spatial downsampling 2. These four layers divide the number of input channels by 2. A spatial average pooling layer then decimates the spatial dimension, and a final (1,1) 2D convolution regress the mean and log standard deviation of the distribution in $\mathbb{R}^L \times \mathbb{R}^L$ with $L = 32$.

Future prediction. The future prediction module is made of the following structure repeated three times: a convolutional Gated Recurrent Unit [4] followed by 3 residual blocks with kernel size $(3, 3)$.

Future instance segmentation and motion decoder. The decoder has a shared backbone and multiple output heads to predict centerness, offset, segmentation and flow. The shared backbone contains:

- a 2D convolution with output channel 64 and stride 2.
- the following block repeated three times: four 2D residual convolutions with kernel size (3, 3). The respective output channels are [64, 128, 256] and strides [1, 2, 2].
- three upsampling layers of factor 2, with skip connections and output channel 64.

Each head is then the succession two 2D convolutions outputting the required number of channels.

B.2. Labels generation

We compute instance center labels as a 2D Gaussian centered at each instance center of mass with standard deviation $\sigma_x = \sigma_y = 3$. The centerness label indicates the likelihood of a pixel to be the center of an instance and is a $\mathbb{R}^{1\times H\times W}$ tensor. For all pixels belonging to a given instance, we calculate the offset labels as the vector pointing to the instance center of mass (a $\mathbb{R}^{2\times H\times W}$ tensor). Finally, we obtain future flow labels (a $\mathbb{R}^{2\times H\times W}$ tensor) by comparing the position of the instance centers of gravity between two consecutive timesteps.

We use the *vehicles* category to obtain 3D bounding boxes of road agents on both the NuScenes and Lyft datasets.

We report results on the official NuScenes validation split. Since the Lyft dataset does not provide a validation set, we create one by selecting random scenes from the dataset so that it contains roughly the same number of samples (6,174) as NuScenes (6,019).

References

[1] Alexandre Alahi, Kratarth Goel, Vignesh Ramanathan, Alexandre Robicquet, Li Fei-Fei, and Silvio Savarese. Social lstm: Human trajectory prediction in crowded spaces. In *Proceedings of the IEEE conference on computer vision and pattern recognition*, pages 961–971, 2016.

[2] Vijay Badrinarayanan Alex Kendall and Roberto Cipolla. Bayesian segnet: Model uncertainty in deep convolutional encoder-decoder architectures for scene understanding. In *Proceedings of the British Machine Vision Conference (BMVC)*, 2017.

[3] Mohammad Babaeizadeh, Chelsea Finn, Dumitru Erhan, Roy H. Campbell, and Sergey Levine. Stochastic variational video prediction. In *Proceedings of the International Conference on Learning Representations (ICLR)*, 2018.

[4] Nicolas Ballas, Li Yao, Chris Pas, and Aaron Courville. Delving deeper into convolutional networks for learning video representations. In *Proceedings of the International Conference on Learning Representations (ICLR)*, 2016.

[5] Holger Caesar, Varun Bankiti, Alex H. Lang, Sourabh Vora, Venice Erin Liong, Qiang Xu, Anush Krishnan, Yu Pan, Giancarlo Baldan, and Oscar Beijbom. nuscenes: A multimodal dataset for autonomous driving. *arXiv preprint arXiv:1903.11027*, 2019.

[6] Sergio Casas, Cole Gulino, Renjie Liao, and Raquel Urtasun. Spatially-aware graph neural networks for relational behavior forecasting from sensor data, 2019.

[7] Sergio Casas, Wenjie Luo, and Raquel Urtasun. Intentnet: Learning to predict intention from raw sensor data. volume 87 of *Proceedings of Machine Learning Research*, pages 947–956. PMLR, 29–31 Oct 2018.

[8] Yuning Chai, Benjamin Sapp, Mayank Bansal, and Dragomir Anguelov. Multipath: Multiple probabilistic anchor trajectory hypotheses for behavior prediction. In Leslie Pack Kaelbling, Danica Kragic, and Komei Sugiura, editors, *Proceedings of the Conference on Robot Learning*, volume 100 of *Proceedings of Machine Learning Research*, pages 86–99. PMLR, 30 Oct–01 Nov 2020.

[9] Bowen Cheng, Maxwell D. Collins, Yukun Zhu, Ting Liu, Thomas S. Huang, Hartwig Adam, and Liang-Chieh Chen. Panoptic-deeplab: A simple, strong, and fast baseline for bottom-up panoptic segmentation. In *Proceedings of the IEEE Conference on Computer Vision and Pattern Recognition (CVPR)*, 2020.

[10] Henggang Cui, Vladan Radosavljevic, Fang-Chieh Chou, Tsung-Han Lin, Thi Nguyen, Tzu-Kuo Huang, Jeff Schneider, and Nemanja Djuric. Multimodal trajectory predictions for autonomous driving using deep convolutional networks. In *2019 International Conference on Robotics and Automation (ICRA)*, pages 2090–2096. IEEE, 2019.

[11] Nemanja Djuric, Henggang Cui, Zhaoen Su, Shangxuan Wu, Huahua Wang, Fang-Chieh Chou, Luisa San Martin, Song Feng, Rui Hu, Yang Xu, Alyssa Dayan, Sidney Zhang, Brian C. Becker, Gregory P. Meyer, Carlos Vallespi-Gonzalez, and Carl K. Wellington. Multixnet: Multiclass multistage multimodal motion prediction, 2020.

[12] Nemanja Djuric, Vladan Radosavljevic, Henggang Cui, Thi Nguyen, Fang-Chieh Chou, Tsung-Han Lin, Nitin Singh, and Jeff Schneider. Uncertainty-aware short-term motion prediction of traffic actors for autonomous driving. In *The IEEE Winter Conference on Applications of Computer Vision*, pages 2095–2104, 2020.

[13] David Ferguson, Michael Darms, Chris Urmson, and Sascha Kolski. Detection, prediction, and avoidance of dynamic obstacles in urban environments. In *2008 IEEE Intelligent Vehicles Symposium*, pages 1149–1154, 2008.

[14] Paolo Fiorini and Zvi Shiller. Motion planning in dynamic environments using velocity obstacles. *The International Journal of Robotics Research*, 17(7):760–772, 1998.

[15] Thierry Fraichard and Hajime Asama. Inevitable collision states. a step towards safer robots? In *Proceedings of the IEEE/RSJ International Conference on Intelligent Robots and Systems (IROS)*, volume 1, pages 388–393, 2003.

[16] Jiyang Gao, Chen Sun, Hang Zhao, Yi Shen, Dragomir Anguelov, Congcong Li, and Cordelia Schmid. Vectornet: Encoding hd maps and agent dynamics from vectorized representation. In *Proceedings of the IEEE/CVF Conference on Computer Vision and Pattern Recognition*, pages 11525–11533, 2020.

[17] Rick Groenendijk, Sezer Karaoglu, T. Gevers, and Thomas Mensink. On the benefit of adversarial training for monocular depth estimation, 2020.

[18] Kaiming He, Xiangyu Zhang, Shaoqing Ren, and Jian Sun. Deep residual learning for image recognition. In *Proceedings of the IEEE Conference on Computer Vision and Pattern Recognition (CVPR)*, 2016.

[19] Noureldin Hendy, Cooper Sloan, Feng Tian, Pengfei Duan, Nick Charchut, Yuesong Xie, Chuang Wang, and James Philbin. Fishing net: Future inference of semantic heatmaps in grids. In *Proceedings of the IEEE Conference on Computer Vision and Pattern Recognition, workshop (CVPRw)*, 2020.

[20] Joey Hong, Benjamin Sapp, and James Philbin. Rules of the road: Predicting driving behavior with a convolutional model of semantic interactions. In *Proceedings of the IEEE Conference on Computer Vision and Pattern Recognition*, pages 8454–8462, 2019.

[21] Anthony Hu, Fergal Cotter, Nikhil Mohan, Corina Gurau, and Alex Kendall. Probabilistic future prediction for video scene understanding. In *Proceedings of the European Conference on Computer Vision (ECCV)*, 2020.

[22] Max Jaderberg, Karen Simonyan, Andrew Zisserman, and Koray Kavukcuoglu. Spatial transformer networks. In *Advances in Neural Information Processing Systems (NeurIPS)*, NIPS'15, pages 2017–2025, Cambridge, MA, USA, 2015. MIT Press.

[23] Xiaojie Jin, Huaxin Xiao, Xiaohui Shen, Jimei Yang, Zhe Lin, Yunpeng Chen, Zequn Jie, Jiashi Feng, and Shuicheng Yan. Predicting scene parsing and motion dynamics in the future. In *Advances in Neural Information Processing Systems*, pages 6915–6924, 2017.

[24] Alex Kendall, Yarin Gal, and Roberto Cipolla. Multi-task learning using uncertainty to weigh losses for scene geome-

try and semantics. In *Proceedings of the IEEE Conference on Computer Vision and Pattern Recognition (CVPR)*, 2018.

[25] R. Kesten, M. Usman, J. Houston, T. Pandya, K. Nadhamuni, A. Ferreira, M. Yuan, B. Low, A. Jain, P. Ondruska, S. Omari, S. Shah, A. Kulkarni, A. Kazakova, C. Tao, L. Platinsky, W. Jiang, and V. Shet. Lyft level 5 perception dataset 2020, 2019.

[26] Dahun Kim, Sanghyun Woo, Joon-Young Lee, and In So Kweon. Video panoptic segmentation. In *Proceedings of the IEEE Conference on Computer Vision and Pattern Recognition (CVPR)*, 2020.

[27] H. W. Kuhn and Bryn Yaw. The hungarian method for the assignment problem. *Naval Res. Logist. Quart*, 1955.

[28] Namhoon Lee, Wongun Choi, Paul Vernaza, Christopher Bongsoo Choy, Philip H. S. Torr, and Manmohan Krishna Chandraker. DESIRE: distant future prediction in dynamic scenes with interacting agents. *Proceedings of the IEEE Conference on Computer Vision and Pattern Recognition (CVPR)*, 2017.

[29] Ming Liang, Bin Yang, Shenlong Wang, and Raquel Urtasun. Deep continuous fusion for multi-sensor 3d object detection. In *Proceedings of the European Conference on Computer Vision (ECCV)*, pages 641–656, 2018.

[30] Chenyang Lu, Marinus Jacobus Gerardus van de Molengraft, and Gijs Dubbelman. Monocular Semantic Occupancy Grid Mapping With Convolutional Variational Encoder-Decoder Networks. *IEEE Robotics and Automation Letters*, 2019.

[31] Pauline Luc, Natalia Neverova, Camille Couprie, Jacob Verbeek, and Yann LeCun. Predicting deeper into the future of semantic segmentation. In *Proceedings of the International Conference on Computer Vision (ICCV)*, 2017.

[32] Wenjie Luo, Bin Yang, and Raquel Urtasun. Fast and furious: Real time end-to-end 3d detection, tracking and motion forecasting with a single convolutional net. In *Proceedings of the IEEE Conference on Computer Vision and Pattern Recognition (CVPR)*, June 2018.

[33] Mong H. Ng, Kaahan Radia, Jianfei Chen, Dequan Wang, Ionel Gog, and Joseph E. Gonzalez. Bev-seg: Bird's eye view semantic segmentation using geometry and semantic point cloud, 2020.

[34] B. Paden, M. Čáp, S. Z. Yong, D. Yershov, and E. Frazzoli. A survey of motion planning and control techniques for self-driving urban vehicles. *IEEE Transactions on Intelligent Vehicles*, 1(1):33–55, 2016.

[35] Bowen Pan, Jiankai Sun, Ho Yin Tiga Leung, Alex Andonian, and Bolei Zhou. Cross-view semantic segmentation for sensing surroundings. *IEEE Robotics and Automation Letters*, 5(3):4867–4873, Jul 2020.

[36] Tung Phan-Minh, Elena Corina Grigore, Freddy A Boulton, Oscar Beijbom, and Eric M Wolff. Covernet: Multimodal behavior prediction using trajectory sets. In *Proceedings of the IEEE/CVF Conference on Computer Vision and Pattern Recognition*, pages 14074–14083, 2020.

[37] Jonah Philion and Sanja Fidler. Lift, splat, shoot: Encoding images from arbitrary camera rigs by implicitly unprojecting to 3d. In *Proceedings of the European Conference on Computer Vision (ECCV)*, 2020.

[38] Nicholas Rhinehart, Rowan McAllister, Kris M. Kitani, and Sergey Levine. PRECOG: prediction conditioned on goals in visual multi-agent settings. *Proceedings of the International Conference on Computer Vision (ICCV)*, 2019.

[39] Thomas Roddick and Roberto Cipolla. Predicting semantic map representations from images using pyramid occupancy networks. In *Proceedings of the IEEE Conference on Computer Vision and Pattern Recognition (CVPR)*, 2020.

[40] Thomas Roddick, Alex Kendall, and Roberto Cipolla. Orthographic feature transform for monocular 3d object detection. In *BMVC*, 2019.

[41] Christian Rupprecht, Iro Laina, Robert Dipietro, Maximilian Baust, Federico Tombari, Nassir Navab, and Gregory D. Hager. Learning in an uncertain world: Representing ambiguity through multiple hypotheses. In *Proceedings of the International Conference on Computer Vision (ICCV)*, 2017.

[42] Avishar Saha, Oscar Mendez, Chris Russell, and Richard Bowden. Enabling spatio-temporal aggregation in birds-eye-view vehicle estimation. In *Proceedings of the International Conference on Robotics and Automation (ICRA)*, 2021.

[43] Meet Shah, Zhiling Huang, Ankit Laddha, Matthew Langford, Blake Barber, Sidney Zhang, Carlos Vallespi-Gonzalez, and Raquel Urtasun. Liranet: End-to-end trajectory prediction using spatio-temporal radar fusion, 2020.

[44] Gabor J. Szekely and Maria L. Rizzo. The energy of data. *Annual Review of Statistics and Its Application*, 4(1):447–479, 2017.

[45] Mingxing Tan and Quoc Le. EfficientNet: Rethinking model scaling for convolutional neural networks. In *Proceedings of the International Conference on Machine Learning (ICML)*, 2019.

[46] Charlie Tang and Russ R Salakhutdinov. Multiple futures prediction. In *Advances in Neural Information Processing Systems*, pages 15424–15434, 2019.

[47] Dequan Wang, Coline Devin, Qi-Zhi Cai, Philipp Krähenbühl, and Trevor Darrell. Monocular plan view networks for autonomous driving. In *2019 IEEE/RSJ International Conference on Intelligent Robots and Systems (IROS)*, pages 2876–2883. IEEE, 2019.

[48] Yan Wang, Wei-Lun Chao, Divyansh Garg, Bharath Hariharan, Mark Campbell, and Kilian Q Weinberger. Pseudo-lidar from visual depth estimation: Bridging the gap in 3d object detection for autonomous driving. In *Proceedings of the IEEE Conference on Computer Vision and Pattern Recognition*, pages 8445–8453, 2019.

[49] Pengxiang Wu, Siheng Chen, and Dimitris N Metaxas. Motionnet: Joint perception and motion prediction for autonomous driving based on bird's eye view maps. In *Proceedings of the IEEE/CVF Conference on Computer Vision and Pattern Recognition*, pages 11385–11395, 2020.

[50] Danfei Xu, Dragomir Anguelov, and Ashesh Jain. Pointfusion: Deep sensor fusion for 3d bounding box estimation. In *Proceedings of the IEEE Conference on Computer Vision and Pattern Recognition*, pages 244–253, 2018.

[51] Xinge Zhu, Zhichao Yin, Jianping Shi, Hongsheng Li, and Dahua Lin. Generative adversarial frontal view to bird view synthesis. In *2018 International conference on 3D Vision (3DV)*, pages 454–463. IEEE, 2018.